Cellulose (2023) 30:7779–7790
https://doi.org/10.1007/s10570-023-05342-1

ORIGINAL RESEARCH

Cellulose acetate for a humidity-responsive self-actuator bilayer composite

Shiva Khoshtinat · Valter Carvelli · Claudia Marano

Received: 10 January 2023 / Accepted: 18 June 2023 / Published online: 5 July 2023

Abstract The use of stimuli-responsive polymers to produce environmentally responsive self-actuators continues to rise. Highly hygroscopic materials are attracting great interest for the design of humidity-responsive self-actuators. In this context, bilayer composites, formed by the coupling of a hygroscopic layer with a non-hygroscopic one, are relevant as they allow for the response to be tuned through the design of the composite layers. Therefore, the meticulous material characterization and the definition of descriptive models of their hygroscopic behavior are the primary steps towards the development of humidity-responsive self-actuators. This study is aimed at measuring and predicting the response of a bilayer composite made of a hygroscopic material layer and a layer of a non-hygroscopic material when subjected to changes in environmental humidity levels, to be used as a humidity-responsive self-actuator. A cellulose acetate was used as the hygroscopic material. Predictions for the induced hygroscopic deformation in the bilayer composite, based on two-physics finite element simulations, are compared to experimental measurements.

Keywords Humidity-responsive composite · Self-actuator · Cellulose acetate · Experimental characterization · Finite element model

Supplementary Information The online version contains supplementary material available at https://doi.org/10.1007/s10570-023-05342-1.

S. Khoshtinat · C. Marano (✉)
Department of Materials, Chemistry and Chemical Engineering "Giulio Natta", Politecnico di Milano, Milan, Italy
e-mail: claudia.marano@polimi.it

V. Carvelli
Department of Architecture, Built Environment and Construction Engineering, Politecnico di Milano, Milan, Italy

Introduction

Stimuli-responsive polymers (SRPs) have emerged as materials to be exploited in the development of a new generation of stimuli-responsive actuators that do not require sensors or processors (Zhang and Serpe 2017; Hu et al. 2020; Wang et al. 2022). In this context, the design of humidity-responsive self-actuators with hygroscopic materials (Okuzaki and Kunugi 1996; Burgert and Fratzl 2009; Shen et al. 2010; Okuzaki et al. 2013; Ma et al. 2013; Rubinger et al. 2013; Ochoa et al. 2013; Ionov 2014; Reichert et al. 2015; Taccola et al. 2015; Yao et al. 2015; Holstov et al. 2015a; Barozzi et al. 2016; Wang et al. 2016, 2017; Weng et al. 2016; Jian et al. 2017; Castaldo et al. 2019; Dingler et al. 2021; Si et al. 2022) to mimic the humidity-induced actuation of plants is not an exception (Burgert and Fratzl 2009; Reyssat and Mahadevan 2009; Reichert et al. 2015; Holstov et al. 2015a; Dingler et al. 2021). Some studies have already used a bilayer composite coupling a hygroscopic material and

a non-hygroscopic one to exploit the different dimensional variations of the two layers induced by a change in the environmental humidity. However, for some of the hygroscopic materials reported in the literature, the moisture absorption and desorption processes differ significantly at the same temperature, and the desorption process is commonly quickened by heating (Greco et al. 2011; Zhou et al. 2014; Taccola et al. 2015; Dingler et al. 2021; Rivadeneyra et al. 2021).

A bilayer composite humidity-responsive actuator, schematically drawn in Fig. 1, exploits the significant length variation of the thin hygroscopic material layer (active layer), caused by a variation in the environmental humidity level, while the non-hygroscopic material substrate (passive layer) has a negligible length variation compared to the active one. If the active layer is constrained on one side by the passive one, the mismatch in deformation results in bending of the bi-layered composite.

The bending effect is similar to that of bi-metal strips under heating described by Timoshenko (1925), which is based on Stoney's work on induced stress in metallic films (Stoney 1909). Berry and Pritchet (1984) showed how Timoshenko's bi-metal strip bending theory can be adapted to describe moisture-induced deformation in a bilayer composite. The bending radius induced by a change in relative humidity, can be estimated by Eq. (1)(Berry and Pritchet 1984), in which the coefficient of hygroscopic expansion (α) and moisture concentration variation (ΔC) are used in place of the coefficient of thermal expansion (CTE) and temperature variation, respectively.

where $\Delta\alpha$ is the difference between the coefficient of hygroscopic expansion of the active layer material (subscript a) and that of the passive one (subscript p) ($\Delta\alpha = \alpha_a - \alpha_p \neq 0$) and h_{tot} is the thickness of the bilayer composite ($h_{tot} = h_a + h_p$). $f(m, n)$ is a function of the layers thicknesses ($m = h_p/h_a$), materials elastic modulus (E), and Poisson ratio (ν) ($n = \frac{\acute{E}_p}{\acute{E}_a}$, where $\acute{E}_a = \frac{E_a}{(1-\nu_a)}$ and $\acute{E}_p = \frac{E_p}{(1-\nu_p)}$). In brief, the induced bending curvature of a bilayer composite is a function of the environmental conditions (relative humidity), the geometry of each layer (thickness), as well as the mechanical and hygroscopic properties of the materials. The thickness of each layer can be designed according to the requirements of each bilayer product in relation to the properties of the hygroscopic material, namely Young's modulus (E_a) and coefficient of hygroscopic expansion (α_a).

Most of the literature, dedicated to the characterization of bilayer humidity-responsive self-actuator composites, considers Eq. (1)—or an adapted analytical model—to evaluate the bending curvature at equilibrium conditions for changes in relative humidity. Some studies (Holstov et al. 2015b; Wang et al. 2017; Abdelmohsen 2019) compare only the initial shape and the final deformation of the bilayer at the equilibrium state, when the actuator is fully saturated and does not deform anymore. Other studies, however, took a step forward by experimentally characterizing the evolution of the bending curvature as a function of time using Eq. (1) (Reyssat and Mahadevan 2009; Yao et al. 2015; Holstov

$$\frac{1}{R} = \kappa = \frac{\Delta\alpha\Delta C f(m,n)}{h_{tot}}, \quad f(m,n) = \frac{6(1+m)^2}{3(1+m)^2 + (1+mn)(m^2 + \frac{1}{m})} \tag{1}$$

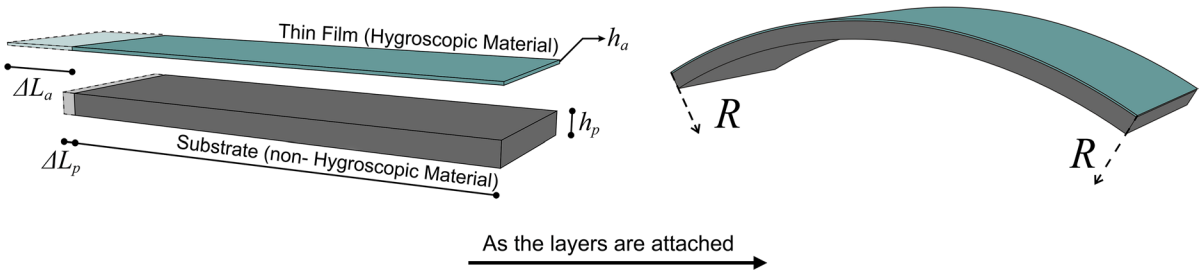

Fig. 1 Schematic representation of humidity-induced bending of a bilayer composite (Berry and Pritchet 1984). ΔL_a and ΔL_p indicate the linear expansion of active and passive layers due to an increase in the environmental humidity level, respectively. h_a and h_p indicate the thickness of active and passive layers, respectively ($h_a < h_p$). R represents the radius of curvature

et al. 2015a). Nonetheless, neglecting the kinetics of moisture or water diffusion leads to uncertainty about the time for the diffusion process to reach the concentration at saturation (equilibrium state).

Considering the authors' previous publications on the characterization and modeling of moisture diffusion (Khoshtinat et al. 2021) and hygroscopic strain induced by moisture absorption (Khoshtinat et al. 2022) of cellulose acetate membranes, this study is dedicated to the characterization and finite element modeling of a humidity-responsive self-actuator bilayer composite made of a cellulose acetate membrane and a non-hygroscopic ply. To the best of the authors' knowledge, no systematic study on the bending curvature evolution in time, accompanied by the relevant finite element modeling of a bilayer composite actuator, has been presented in the literature. In particular, there seems to be no study that includes highly hygroscopic materials such as cellulose acetate, which respond quickly to both increases and decreases in the environment's relative humidity. The finite element model presented in this study reproduces the peculiar hygroscopic behavior of cellulose acetate by using experimentally characterized material features, i.e., coupling the moisture diffusion process and the relevant induced deformation of a cellulose acetate membrane, while available analytical models (Yoon et al. 2007; Wong 2010) reformulate heat transfer theoretical models by just substituting thermal features with the diffusion counterparts.

A summary of previously characterized features of the cellulose acetate membrane employed in this study is presented first. Then, the experimental results of the bending curvature evolution induced by humidity variation in the cellulose acetate-based self-actuator composite are described. Finally, the two-physics finite element modelling is detailed, and the experimental data are compared to numerical predictions and to the commonly adopted analytical model (Eq. (1)).

Materials and experimental procedures

Cellulose acetate membrane

Mazzucchelli 1849 S.p.A. supplied cellulose acetate (CA) powder (53.3% acetylation). A 20% w/w solution of Cellulose Acetate was prepared by gradually adding the CA powder to ethyl lactate (≥98% purity, acquired from Sigma-Aldrich). An RCT basic IKAMAGTM safety control magnetic stirrer was used to mix the solution at 80 °C for 90 min (300 rpm), followed by another 90 min at 80 °C (200 rpm). The solution was poured onto a glass substrate after reaching room temperature, and a film of about 500 µm thickness was cast by a K Control Coater. First, the cast solution was placed in a closed container with no air flow for 3 h to limit solvent evaporation at the beginning of the drying process and to avoid the creation of bubbles. It was then dried for 4 h in a Vuotest Mazzali vacuum oven to speed up solvent evaporation. Finally, the CA membranes were peeled from the glass substrate and dried for 24 h at 125 °C in an oven (Mazzali Thermair) to guarantee full evaporation of any leftover solvent. More details on the process of membrane preparation and the obtained final thicknesses are presented in Khoshtinat et al. (2021, 2022).

Bilayer composite

The bilayer composite was prepared using the previously characterized cellulose acetate membranes as its active layers (Khoshtinat et al. 2021, 2022). The geometry and material characteristics of the passive substrate layer have been selected to fulfill the assumptions of Berry and Pritchet's analytical model (Berry and Pritchet 1984) and to guarantee a valid comparison between the experimental and finite element results with the analytical model. Therefore, the substrate: (1) must be thicker than the CA membrane ($h_p > h_a$), (2) must have a negligible hygroscopic expansion coefficient compared to cellulose acetate ($\alpha_p << \alpha_a$), and (3) must be resistant to humidity with good adhesion to the CA membrane.

High wettability and inherently low surface energy of cellulose-based materials (Heinze et al. 2018), cellulose acetate in our case, lead to a poor interfacial bonding/adhesion. Although treatments such as chemical modification or plasma treatment can increase cellulose acetate's ability to adhere, they might affect the hygroscopic behavior by changing the concentration and/or arrangement of the hydroxyl groups on the membrane surface. Since the goal of this investigation is the characterization of the response of cellulose acetate layered composites to changes in humidity level, rather than the improvement of the CA

adhesion, an adhesive tape (Tesa® 64621) that allows to satisfy all the mentioned requirements was chosen as the substrate. Tesa® 64621 is a double-sided adhesive tape with a PP-carrier and a synthetic rubber adhesive. It is not hygroscopic and ensures very good bonding on polar and non-polar surfaces. Since, the adhesive layer has a low stiffness, the release liner (silicon-coated paper) was preserved, and the two together are considered as a homogeneous material. The Young's modulus of Tesa® 64621, including its release liner, was 4.62 ± 0.03 GPa, measured by uniaxial tensile tests (strain rate 6×10^{-3} min^{-1}, $T = 25 \pm 1$ °C).

As observed in a previous study (Khoshtinat, et al. 2021), cellulose acetate responds quickly to variations in relative humidity. During preliminary attempts, the adhesive tape substrate was coupled to the CA membrane soon after it was removed from the oven (24 h, 125 °C drying procedure). However, due to thermal shrinkage induced by cooling from 125 °C to room temperature and the hygroscopic expansion in the free membrane's surface during the adhesion time (almost 30 s), a curvature was noticed in the composite. This could have been avoided if the composite assembly was carried out in a dry environment; however, such a facility was not available for this study. Therefore, the most practical approach was to couple the layers in a climatized room, at a known relative humidity, once the CA membrane had reached its moisture saturation state. Flat bilayer composites were thus obtained by coupling the passive layer (thickness including the release liner $h_p = 145 \pm 1$ µm) with a cellulose acetate membrane ($h_a = 86 \pm 3$ µm) equilibrated in the climatized room at a temperature (T) of 25 °C and a relative humidity (RH) of 35%. Specimens of 60×12.5 mm^2 were then hollow punched, and the bending induced by changes in RH was measured in different ranges (see Table 1).

Experimental setup and image analysis

The bending deformation of the bilayer composite induced by a change in the relative humidity was measured using digital images recorded at a predefined frequency, which followed an extensively used approach (Reyssat and Mahadevan 2009; Correa et al. 2015; Holstov et al. 2015a; Vailati et al. 2018; Abdelmohsen et al. 2018, 2019; Abdelmohsen 2019). Specimens previously equilibrated at 17% and 35% of RH were placed within a polymethylmethacrylate closed chamber designed and built to have a constant humidity environment. Levels of relative humidity between 77 and 80% were obtained inside the chamber at room temperature ($T = 25$ °C), by using salt solutions of sodium chloride in distilled water (about 2/1 w/w). To stabilize the relative humidity, the salt solution was placed in the chamber 72 h in advance. The humidity level of 17% was obtained with a silica-gel desiccator. An RH level of 35% was, as already stated, the humidity in the laboratory thermostatic room. Three specimens, obtained from three different cellulose acetate membranes with the same thickness of about 86 ± 3 µm, were tested to assess the reproducibility, as detailed in Table 1.

Figure 2 depicts a schematic representation of the experimental setup for image acquisition at a constant relative humidity and temperature ($T = 25$ °C). The specimen (60 mm long) was clamped between two metal supports, leaving an overhanging length of 40 or 50 mm and placed in front of a vertical grid paper.

Table 1 Specimen dimensions and experimental conditions

Specimen	Length L*, ** (mm)	Active layer thickness h_a** (mm)	Passive layer thickness h_p** (mm)	Width W** (mm)	*RH* (%)	
					From	To
S1	50	0.086 ± 0.003	0.145 ± 0.001	12.5	17	80
					35	
S2	40				35	77
S3	40				17	77
					35	
					35	80

*Free length of the specimen (or overhanging length)

**Measured at 25 °C and $RH = 35\%$

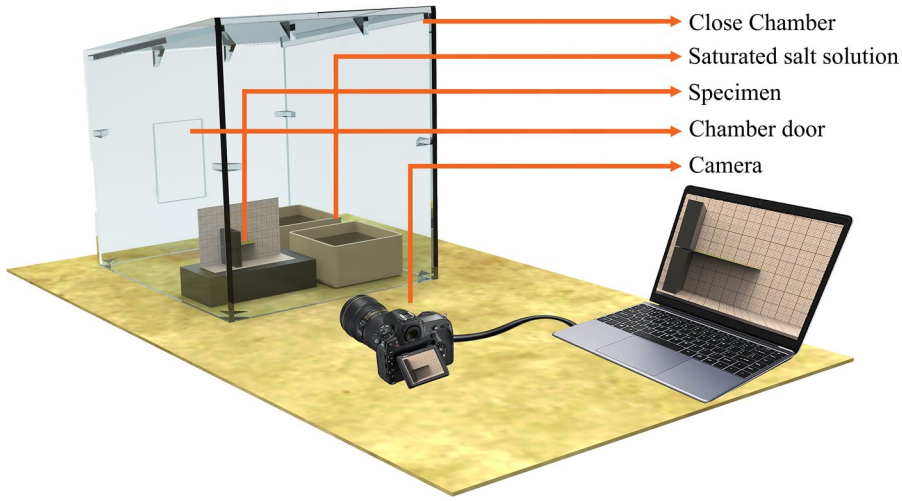

Fig. 2 Schematic representation of the experimental setup

The procedure of setting the specimen in the chamber takes about one minute. A digital camera (Nikon D70) was positioned perpendicular to the grid paper, at a distance of about 50 cm from the specimen. The time required for a 86 µm thick membrane of dry cellulose acetate ($RH = 0\%$) to reach saturation at a relative humidity of 80%, calculated by the finite element simulation presented in authors' previous work (Khoshtinat et al. 2021), is about 60 min when the absorption occurs from only one of its surfaces. Considering the climatized room's relative humidity ($RH = 35\%$) and the fact that the cellulose acetate membrane is not dry, a longer duration for the experimental procedure was hypothesized; therefore, the evolution of the bending of the self-actuator bilayer composite was tracked for 100 min. The camera used had a frequency acquisition rate of 0.016 Hz (one image every minute). The video showing the experimentally recorded bending deformation of specimen S1 with humidity variation from 35 to 80% is available as Online Resource 1.

Figure 3 shows, as an example, the image of specimen *S1* equilibrated at a relative humidity of 80% and the reference system for the measurement of the curvature. The recorded digital images were imported into Rhinoceros® as a picture frame for post-processing. Beside the main bending, a minor twist of the specimen was noted (Fig. 3), which could have been

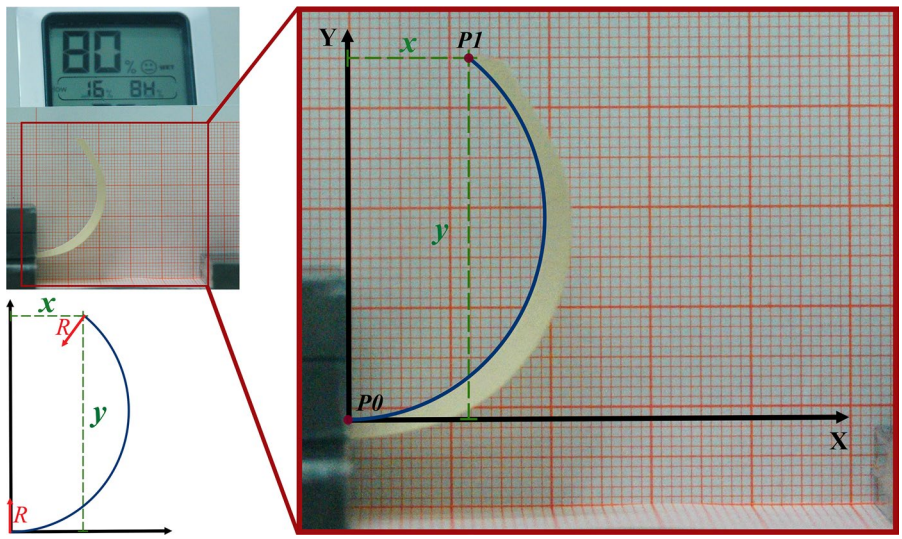

Fig. 3 Bilayer composite prepared at $RH = 35\%$ and kept for 100 min in the closed chamber at a relative humidity of 80%. The reference system used to evaluate the curvature of the *P0–P1* arc is also shown

motivated by 3 μm variation in the thickness of the CA membrane. To neglect this small twist, the origin of the X–Y reference frame was set at the clamp between the metal supports (*P0*), and the bent shape of the specimen was fitted with an arc of a circumference from point *P0* to point *P1* positioned on the specimen side closest to the camera (Fig. 3), setting $tan(P0)=0$. The bending curvature (κ) was obtained by Eq. (2), where x and y are the coordinates of *P1*. This process was performed on all the collected frames for each specimen.

$$\kappa = \frac{1}{R} = \frac{2x}{y^2 + x^2} \tag{2}$$

Finite element modelling

Finite element simulations were performed by COMSOL Multiphysics® 5.6. Figure 4 depicts some features of the adopted finite element model. In the numerical analyses, three geometric parameters have been kept constant, namely the width ($W=12.5$ mm) and the active and passive layers' thicknesses ($h_a=0.086$ mm, $h_p=0.145$ mm). The length (L) has been varied based on the overhanging length of each specimen (Table 1). The concentration at saturation (C_{sat} (g mm^{-3})) has been defined as a function of relative humidity by Eq. (3), according to the previous research (Khoshtinat et al. 2022).

$$C_{sat} = 1.19 \times 10^{-10} \times RH^3 - 7.97 \times 10^{-9} \times RH^2 + 8.09 \times 10^{-7} \times RH \tag{3}$$

Two 3D prismatic layers have been defined, one for the passive substrate ($L \times W \times h_p$) and the other for the cellulose acetate membrane ($L \times W \times h_a$). The two layers have been considered perfectly bonded by a tie constraint to guarantee continuity at the interface. Two user-defined materials have been set using the material properties in Table 2, where ρ, E, ν, β and D are: density, Young's modulus, Poisson's ratio, relaxation factor, and diffusion coefficient, respectively. As previously mentioned, the mechanical properties are supposed to be insensitive to relative humidity. This hypothesis might not be realistic for some hygroscopic materials, and it will be topic for future developments of the present study.

The coefficient of hygroscopic expansion (α) for cellulose acetate has been defined as a function of relative humidity (RH) according to Eq. (4) (Khoshtinat et al. 2021).

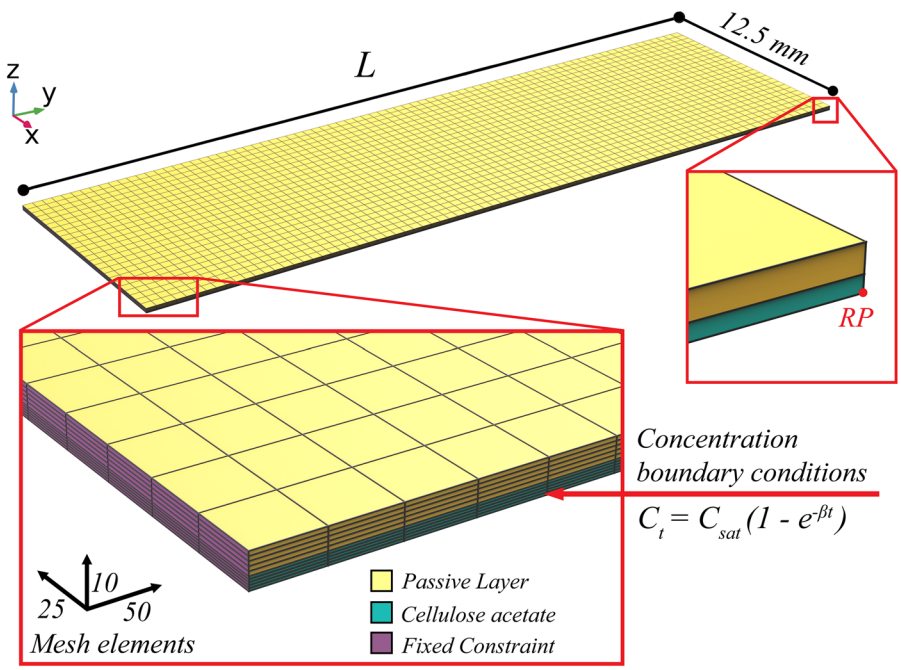

Fig. 4 Some features of the finite element model

Table 2 Materials properties used for the finite element simulations

Materials	ρ (g cm^{-3})	E (GPa)	ν (–)	β (s^{-1})	D (mm^2 s^{-1})
Cellulose acetate	1.3 (Wypych 2016)	1.1 (Khoshtinat et al. 2022)	0.39 (Wypych 2016)	0.026 (Khoshtinat et al. 2021)	3.35×10^{-06} (Khoshtinat et al. 2021)
Tesa® 64621	1.35	4.64	0.33	–	–

$$\alpha = \frac{803 \times RH^2 - 51400 \times RH + 1.16 \times 10^6}{1.19 \times RH^2 - 79.7 \times RH + 8090} \quad (4)$$

The bending deformation of the self-actuator bilayer composite is caused by a mismatch between the mechanical properties and the linear hygroscopic expansion of the active layer (cellulose acetate) and the passive layer ($\varepsilon_{hygro(passive)}=0$). Since the passive layer is a non-hygroscopic material, the input parameters for the diffusion process were set only for the active layer (cellulose acetate membrane) considering its non-Fickian behavior (Khoshtinat et al. 2021). The initial dry condition was assumed to be a null initial moisture concentration, $C_0=0$ g·mm^{-3}. The concentration boundary condition was enforced on the faces of cellulose acetate membrane exposed to the humid environment, as a function of time in Eq. (5) (Khoshtinat et al. 2021).

$$C_t = C_{sat}(1 - e^{-\beta t}) \quad (5)$$

An external face of the model was fixed to reproduce the cantilever, see Fig. 4. From the top face of the passive layer (adhesive tape) to the bottom face of the cellulose acetate membrane, a user-controlled swept mesh was created, forming a discretized volume of $25\times50\times10$ 8-nodes hexahedral elements (total of 12,500 finite elements).

Two separate time-dependent analyses for the diffusion process and hygroscopic swelling were created to minimize computational time compared to a single analysis that included all physical processes. For both analyses, a time range of 100 min was set. First, the diffusion process simulation was run. Then, the hygroscopic swelling was performed, referring to the output of the first analysis and including geometric nonlinearity. The evolution of the bending curvature of the self-actuator composite for the simulated time (100 min) was determined by a built-in function considering the displacement of one external node (*RP* in Fig. 4). The predictions were compared to the experimental results as well as to the analytical model in Eq. (1).

The video showing the prediction of the non-Fickian moisture diffusion and the consequent hygroscopic deformation in the bilayer with humidity variation from 35 to 80% is available in Online Resource 2.

Results and discussion

Figure 5 shows the experimental results of the bending curvature (κ) evolution in time induced by relative humidity variations for specimens first equilibrated at $RH=35\%$ and then placed into the closed chamber at $RH=77\%$ or 80% (see Table 1 for the experimental conditions). As expected,

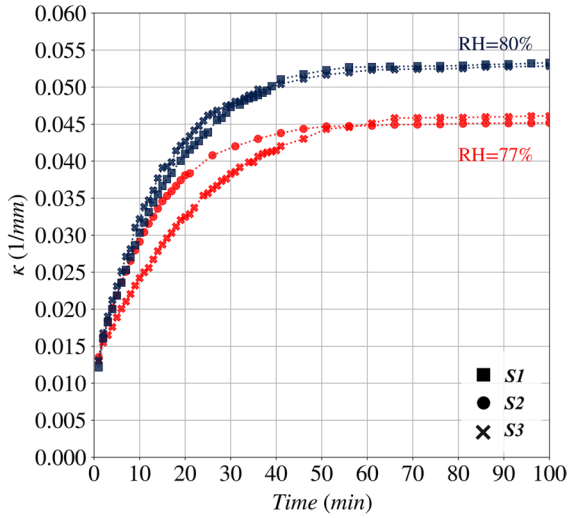

Fig. 5 Experimental results of bending curvature (κ) of self-actuators bilayer composite induced by relative humidity change, from $RH=35\%$ in a climatized room to 77% and 80% in a closed chamber

by increasing the relative humidity, the final induced bending curvature in the bilayer composite increases as well. The initial point of all curves is the curvature of the specimen given by the first image captured by the camera, i.e. after one minute of exposure to a relative humidity of 77% or 80%, as detailed in sub-Sect. 2.3. During the first 20 min, the bending curvature increases rapidly. After this period, the variation of κ as a function of time decreases steadily, up to 40-min mark. Then, between 40 and 60 min, the curvature approaches a plateau. After 60 min, the constant curvature indicates the conclusion of the moisture absorption process. It should be noted that the observed behavior is similar to the trend of time dependency of moisture diffusion (Hansen 2010; Mensitieri and Scherillo 2012), emphasizing the influence of moisture absorption on the bending curvature. Even though three specimens from three different membranes were used and the test was replicated on each one with different conditions, the consistency of the results highlights the good repeatability and reproducibility of the measurements.

To assess the effect of the initial relative humidity on the bending curvature and the cyclic behavior of this self-actuator composite, specimens were partially dried by keeping them for 24 h in a closed chamber containing dried silica gel ($RH = 17\%$). This led to a negative bending curvature of -0.0199, as shown in Fig. 6 (images in center and the first point in the Second cycles graphs). Then, they were immediately put in the closed chamber with higher relative humidity. Figure 6 depicts the results of two specimens, *S1* and *S3*, at relative humidity levels of 80% and 77%, respectively, both starting from 35% *RH* (see Table 1). Figure 6a shows the curvature evolution of specimen *S1*, which was preliminarily equilibrated at $RH = 35\%$ and was: (1) exposed to $RH = 80\%$ for 100 min (first cycle), (2) dried for 24 h at $RH = 17\%$, and (3) exposed again to $RH = 80\%$ for another 100 min (second cycle). Figure 6b reports similar results for specimen *S3*, exposed to a humidity of 77%.

At $RH = 80\%$ for *S1* and $RH = 77\%$ for *S3*, the ultimate bending curvature is consistent regardless of the starting relative humidity (17% or 35%). The starting *RH* influences the bending curvature captured 1 min after exposure. This effect is due to the difference in the initial bending curvature. For the specimen that has been stabilized at $RH = 35\%$, the starting bending curvature was $\kappa = 0$; whereas for the same specimen stabilized at $RH = 17\%$, the starting bending curvature was $\kappa = -0.0199$.

Figure 7a shows the deformation over time of the self-actuator composite due to the moisture absorption simulated by the finite element model for the specimen with the same geometry as *S1* at the relative humidity of 80%. The overlapping of the self-actuator shape after 60 and 70 min indicates that no further deformation occurs during this period, suggesting that the moisture diffusion process in the cellulose acetate membrane has already terminated, as discussed in sub-Sect. 2.3. Simulation also highlights the fast response of the self-actuator composite to changes in relative humidity. The bilayer composite deforms considerably during the first two minutes of exposure to the higher relative humidity level, which points out that this self-actuator can be considered an alternative for applications such as indoor humidity control, as presented in some projects (Reichert et al. 2015; Menges and Reichert 2015; Correa et al. 2015; Holstov et al. 2015a).

The discrepancy between the *S1* specimen's predicted final shape in Fig. 7a and the experimental one (Fig. 3) is mainly due to the preparation of the bilayer composite at the relative humidity of 35%, which imparted a hygroscopic expansion of the cellulose acetate membrane. As mentioned in sub-Sect. 2.2, it was not possible to reach a relative humidity of 0% in the laboratory, and the adhesive tape-based passive layer was coupled to cellulose acetate membrane at 35% *RH*. Since the bending curvature at equilibrium is unaffected by diffusion kinetics, the curvature from dry ($RH = 0\%$) to 80% relative humidity is equal to the sum of the curvatures from dry to 35% and from 35 to 80% (Holstov et al. 2015a). Therefore, the variation of bending curvature from the relative humidity of 35% to 80% ($\Delta\kappa_{RH\,(35–80)}$) can be retrieved as:

$$\Delta\kappa_{RH(35-80)} = \kappa_{RH(0-80)} - \kappa_{RH(0-35)} \tag{6}$$

Figure 7b shows a comparison of the evolution over time of the bending curvature of the experiment and the numerical simulation for the specimen *S1* at 80% *RH*. Moreover, the analytical model prediction for the final bending curvature (Eq. (1)) is compared, assuming the relative humidity dependent coefficient of hygroscopic expansion according to Eq. (4), setting $n = \acute{E}_p/\acute{E}_a = 3.84$, $m = h_p/h_a = 1.69$

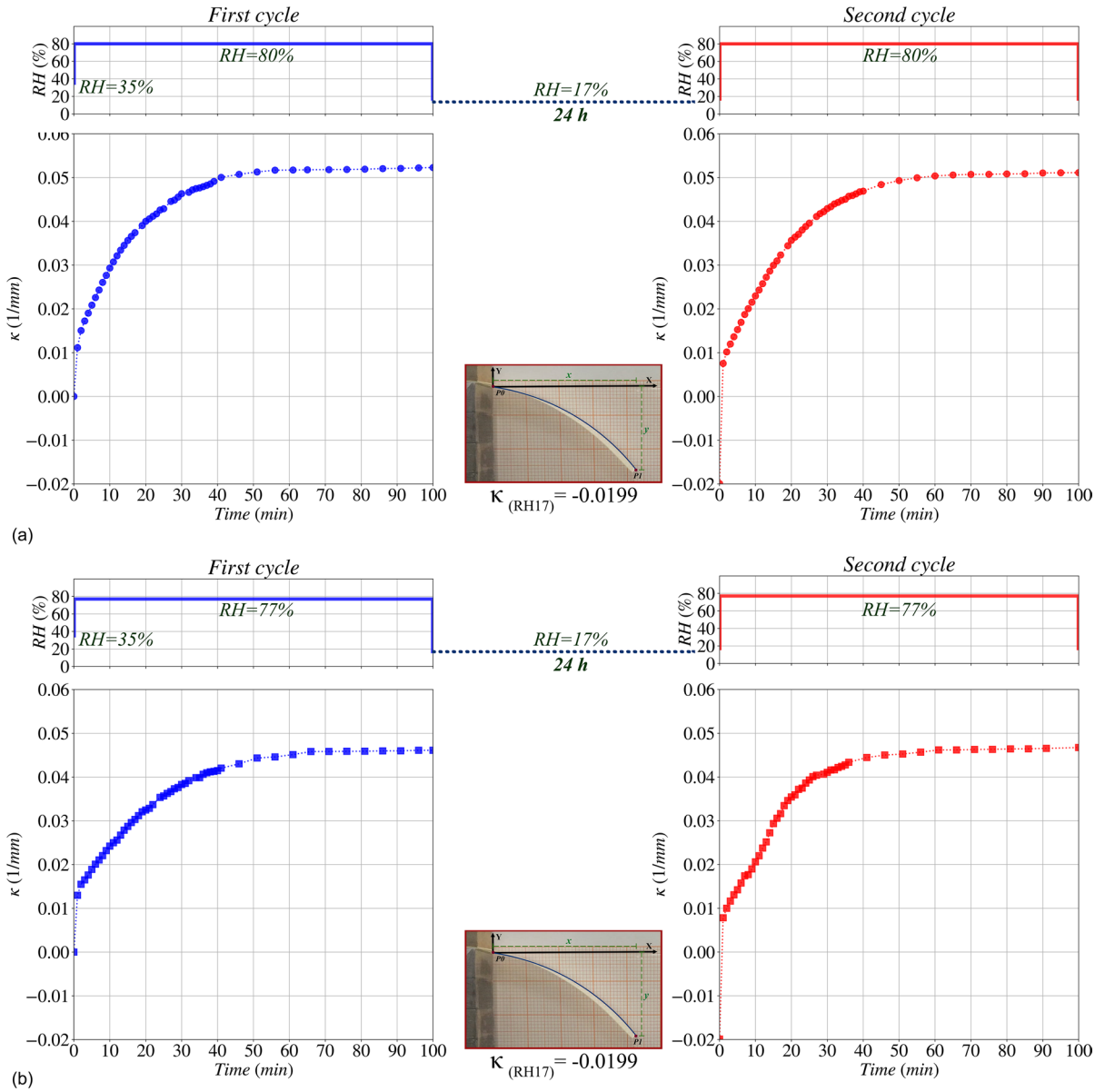

Fig. 6 Experimental results (curvature evolution over time) for an initial relative humidity of **a** 80% and **b** 77%

and $h_{tot}=0.228$ mm (see Tables 1 and 2). Both the numerical and analytical predictions have been adjusted according to Eq. (6). Figure 7b shows a lower rate of growth of experimental bending curvature compared to finite element modeling. This might be related to the experiment's initial condition ($RH=35\%$) and thus the slightly lower diffusion coefficient of the cellulose acetate, since it has been partially plasticized by the absorbed moisture compared to the dry one.

In terms of the ultimate bending curvature, the experimental results ($\kappa=0.0511$ mm^{-1}, $R=19.56$ mm) and the finite element simulation ($\kappa=0.0519$ mm^{-1}, $R=19.26$ mm) are in very good agreement with each other. Bending radius R difference is approximately just 0.3 mm. The analytical model, on the other hand, estimates a final curvature

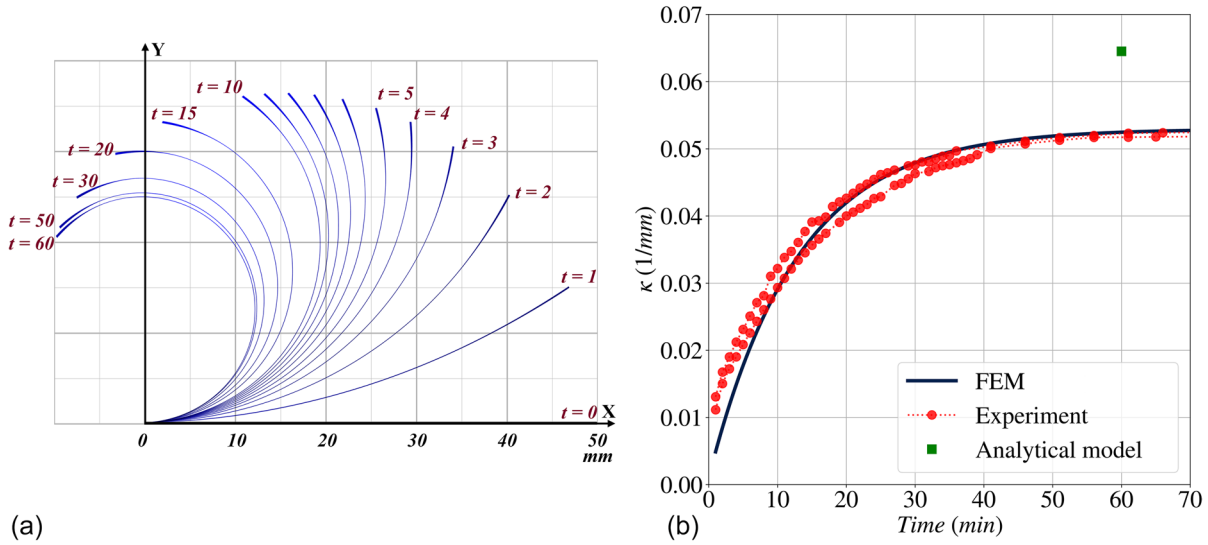

Fig. 7 **a** Self-actuator deformation by finite element simulation, **b** comparison between experimental data, analytical (Eq. (1)), and finite element model (FEM)

of only 0.0645 mm^{-1} (R = 15.5 mm), resulting in a 3.43 mm difference in bending radius from the experiment. The analytical model's curvature overestimation is the result of its simplifications and assumptions. It must be mentioned that the bending curvature in the experiment is also dependent on the plasticization of the cellulose acetate membrane caused by moisture absorption, which results in a decrease of the Young's modulus of the cellulose acetate, which has not been considered in the analytical and numerical models.

Conclusions

A humidity-responsive self-actuator composite, coupling a non-hygroscopic adhesive tape and a cellulose acetate membrane, has been proposed. The experimental setup and procedure for the characterization of the induced bending deformation in the self-actuator bilayer composite have been presented for tests performed at $T = 25 \pm 1$ °C, and at relative humidities of $RH = 17$, 77, and 80%. A finite element model, implementing the peculiar hygroscopic behavior of cellulose acetate, was exploited for predicting the evolution of the non-Fickian moisture diffusion and the relevant induced hygroscopic expansion. Experimentally evaluated material properties, such as the absorbed moisture concentration at saturation (C_{sat}), the hygroscopic strain (ε_{hygro}), the diffusion coefficient (D), and the relaxation factor (β) of the cellulose acetate, among other properties, were used as inputs of the finite element model. Attention was dedicated to the relative humidity level for the bilayer composite preparation and its effect on the self-actuated bending curvature evolution.

The proposed numerical model not only accurately predicts the equilibrium bending curvature, but it also provides the transient bending curvature of the cellulose acetate-based self-actuator composite. The comparison between the numerical model and the experimental measurements also highlights how the experimental initial conditions affect the performance of the self-actuator. The agreement between the experimental measurements and finite element numerical predictions shows the accuracy of the model, which can be adopted for the design and tuning of the proposed hygroscopic self-actuator composite for different applications. Future investigations should be aimed at evaluating the effects of relative humidity and temperature on the plasticization and mechanical properties of the cellulose acetate to improve the accuracy of the finite element model.

Acknowledgments The cellulose acetate powder, used in this study, was kindly supplied by Mazzucchelli 1849 S.p.A. (Italy).

Author contributions SK: Investigation; Conceptualization, Methodology, Data curation, Formal analysis, Validation, Writing—original draft. VC: Investigation; Conceptualization, Supervision, Methodology; Writing—review and editing. CM: Investigation; Conceptualization, Supervision, Methodology, Validation, Writing—review and editing.

Funding Open access funding provided by Politecnico di Milano within the CRUI-CARE Agreement. No funding was received for conducting this study.

Data availability Software application or custom code are available on request.

Declarations

Conflict of interest The authors declare that they have no known competing financial interests or personal relationships that could have appeared to influence the work reported in this paper.

Consent for publication All authors gave explicit consent to publish.

Ethics approval and consent to participate All authors gave explicit consent to participate.

References

Abdelmohsen S (2019) HMTM: Hygromorphic-thermobimetal composites as a novel approach to enhance passive actuation of adaptive façades. In: 18th CAAD Future 2019 international conference

Abdelmohsen S, Massoud P, El-Dabaa R et al (2018) A computational method for tracking the hygroscopic motion of wood to develop adaptive architectural skins. In: Proceedings of the 36th international conference on education and research in computer aided architectural design in Europe, pp 253–262. https://doi.org/10.52842/conf.ecaade.2018.2.253

Abdelmohsen S, Adriaenssens S, Gabriele S et al (2019) Hygroscapes: innovative shape shifting façades. In: Lecture notes in civil engineering. Springer, Cham, pp 675–702. https://doi.org/10.1007/978-3-030-03676-8_26

Barozzi M, Lienhard J, Zanelli A, Monticelli C (2016) The sustainability of adaptive envelopes: developments of kinetic architecture. Procedia Eng 155:275–284. https://doi.org/10.1016/j.proeng.2016.08.029

Berry BS, Pritchet WC (1984) Bending-cantilever method for the study of moisture swelling in polymers. IBM J Res Dev 28:662–667. https://doi.org/10.1147/rd.286.0662

Burgert I, Fratzl P (2009) Actuation systems in plants as prototypes for bioinspired devices. Philos Trans R Soc Math Phys Eng Sci 367:1541–1557. https://doi.org/10.1098/rsta.2009.0003

Castaldo R, Lama GC, Aprea P et al (2019) Humidity-driven mechanical and electrical response of graphene/cloisite hybrid films. Adv Funct Mater 29:1807744. https://doi.org/10.1002/adfm.201807744

Correa D, Papadopoulou A, Guberan C et al (2015) 3D-printed wood: programming hygroscopic material transformations. 3D Print Addit Manuf 2:106–116. https://doi.org/10.1089/3dp.2015.0022

Dingler C, Müller H, Wieland M et al (2021) From understanding mechanical behavior to curvature prediction of humidity-triggered bilayer actuators. Adv Mater 33:2007982. https://doi.org/10.1002/adma.202007982

Greco F, Zucca A, Taccola S et al (2011) Ultra-thin conductive free-standing PEDOT/PSS nanofilms. Soft Matter 7:10642. https://doi.org/10.1039/c1sm06174g

Hansen CM (2010) The significance of the surface condition in solutions to the diffusion equation: explaining "anomalous" sigmoidal, Case II, and Super Case II absorption behavior. Eur Polym J 46:651–662. https://doi.org/10.1016/j.eurpolymj.2009.12.008

Heinze T, El Seoud OA, Koschella A (2018) Cellulose derivatives. Springer, Cham. https://doi.org/10.1007/978-3-319-73168-1

Holstov A, Bridgens B, Farmer G (2015a) Hygromorphic materials for sustainable responsive architecture. Constr Build Mater 98:570–582. https://doi.org/10.1016/j.conbuildmat.2015.08.136

Holstov A, Morris P, Farmer G, Bridgens B (2015b) Towards sustainable adaptive building skins with embedded hygromorphic responsiveness. In: Proceedings of the international conference on building envelope design and technology—advanced building skins, pp 57–67

Hu L, Wan Y, Zhang Q, Serpe MJ (2020) Harnessing the power of stimuli-responsive polymers for actuation. Adv Funct Mater 30:1903471. https://doi.org/10.1002/ADFM.201903471

Ionov L (2014) Hydrogel-based actuators: possibilities and limitations. Mater Today 17:494–503. https://doi.org/10.1016/j.mattod.2014.07.002

Jian M, Wang C, Wang Q et al (2017) Advanced carbon materials for flexible and wearable sensors. Sci China Mater 60:1026–1062. https://doi.org/10.1007/s40843-017-9077-x

Khoshtinat S, Carvelli V, Marano C (2021) Moisture absorption measurement and modelling of a cellulose acetate. Cellulose 28:9039–9050. https://doi.org/10.1007/s10570-021-04114-z

Khoshtinat S, Carvelli V, Marano C (2022) Characterization and modeling the hygroscopic behavior of cellulose acetate membranes. Cellulose 29:2175–2186. https://doi.org/10.1007/s10570-022-04450-8

Ma M, Guo L, Anderson DG, Langer R (2013) Bio-inspired polymer composite actuator and generator driven by water gradients. Science 339:186–189. https://doi.org/10.1126/science.1230262

Menges A, Reichert S (2015) Performative wood: physically programming the responsive architecture of the hygroscope and hygroskin projects. Archit Des 85:66–73. https://doi.org/10.1002/ad.1956

Mensitieri G, Scherillo G (2012) Environmental resistance of high performance polymeric matrices and composites. In: Wiley encyclopedia of composites. Wiley, Hoboken. https://doi.org/10.1002/9781118097298.weoc074

Ochoa M, Chitnis G, Ziaie B (2013) Laser-micromachined cellulose acetate adhesive tape as a low-cost smart material. J Polym Sci Part B Polym Phys 51:1263–1267. https://doi.org/10.1002/polb.23337

Okuzaki H, Kunugi T (1996) Adsorption-induced bending of polypyrrole films and its application to a chemomechanical rotor. J Polym Sci Part B Polym Phys 34:1747–1749. https://doi.org/10.1002/(SICI)1099-0488(19960730)34:10%3c1747::AID-POLB5%3e3.0.CO;2-N

Okuzaki H, Kuwabara T, Funasaka K, Saido T (2013) Humidity-sensitive polypyrrole films for electro-active polymer actuators. Adv Funct Mater 23:4400–4407. https://doi.org/10.1002/adfm.201203883

Reichert S, Menges A, Correa D (2015) Meteorosensitive architecture: biomimetic building skins based on materially embedded and hygroscopically enabled responsiveness. Comput Aided Des 60:50–69. https://doi.org/10.1016/j.cad.2014.02.010

Reyssat E, Mahadevan L (2009) Hygromorphs: from pine cones to biomimetic bilayers. J R Soc Interface 6:951–957. https://doi.org/10.1098/rsif.2009.0184

Rivadeneyra A, Marín-Sánchez A, Wicklein B et al (2021) Cellulose nanofibers as substrate for flexible and biodegradable moisture sensors. Compos Sci Technol 208:108738. https://doi.org/10.1016/j.compscitech.2021.108738

Rubinger C, Calado H, Rubinger R et al (2013) Characterization of a sulfonated polycarbonate resistive humidity sensor. Sensors 13:2023–2032. https://doi.org/10.3390/s130202023

Shen L, Fu J, Fu K et al (2010) Humidity responsive asymmetric free-standing multilayered film. Langmuir 26:16634–16637. https://doi.org/10.1021/la102928g

Si W, Weng Y, Tan B, Zhang S (2022) Adopted ion-pair effect to construct bicontinuous starch-based gel and its application in humidity sensitivity and strain-responsiveness. Compos Part B Eng 234:109696. https://doi.org/10.1016/j.compositesb.2022.109696

Stoney GG (1909) The tension of metallic films deposited by electrolysis. Proc R Soc Lond Ser Contain Pap Math Phys Charact 82:172–175. https://doi.org/10.1098/rspa.1909.0021

Taccola S, Greco F, Sinibaldi E et al (2015) Toward a new generation of electrically controllable hygromorphic soft actuators. Adv Mater 27:1668–1675. https://doi.org/10.1002/adma.201404772

Timoshenko S (1925) Analysis of bi-metal thermostats. J Opt Soc Am 11:233–255. https://doi.org/10.1364/JOSA.11.000233

Vailati C, Bachtiar E, Hass P et al (2018) An autonomous shading system based on coupled wood bilayer elements. Energy Build 158:1013–1022. https://doi.org/10.1016/j.enbuild.2017.10.042

Wang DH, McKenzie RN, Buskohl PR et al (2016) Hygromorphic polymers: synthesis, retro-michael reaction, and humidity-driven actuation of ester–sulfonyl polyimides and thermally derived copolyimides. Macromolecules 49:3286–3299. https://doi.org/10.1021/acs.macromol.6b00250

Wang W, Yao L, Cheng C-Y et al (2017) Harnessing the hygroscopic and biofluorescent behaviors of genetically tractable microbial cells to design biohybrid wearables. Sci Adv 3:1601984. https://doi.org/10.1126/sciadv.1601984

Wang F, Kong Y, Shen F et al (2022) High-performance microfibrillated cellulose-based low voltage electroactive ionic artificial muscles in bioinspired applications. Compos Part B Eng 228:109436. https://doi.org/10.1016/j.compositesb.2021.109436

Weng M, Zhou P, Chen L et al (2016) Multiresponsive bidirectional bending actuators fabricated by a pencil-on-paper method. Adv Funct Mater 26:7244–7253. https://doi.org/10.1002/adfm.201602772

Wong CP (2010) Moisture sensitivity of plastic packages of IC devices. Springer, Boston

Yao L, Ou J, Cheng C-Y et al (2015) bioLogic:natto cells as nanoactuators for shape changing interfaces. In: Proceedings of the 33rd annual ACM conference on human factors in computing systems. ACM, New York, NY, USA, pp 1–10. https://doi.org/10.1145/2702123.2702611

Yoon S, Han B, Wang Z (2007) On moisture diffusion modeling using thermal-moisture analogy. J Electron Packag 129:421–426. https://doi.org/10.1115/1.2804090

Zhang QM, Serpe MJ (2017) Stimuli-Responsive polymers for actuation. ChemPhysChem 18:1451–1465. https://doi.org/10.1002/CPHC.201601187

Zhou J, Anjum DH, Chen L et al (2014) The temperature-dependent microstructure of PEDOT/PSS films: insights from morphological, mechanical and electrical analyses. J Mater Chem C 2:9903–9910. https://doi.org/10.1039/C4TC01593B